

Nanowire Arrays as Force Sensors with Super-Resolved Localization Position Detection: Application to Optical Measurement of Bacterial Adhesion Forces

Aldeliane M. da Silva, Prasana K. Sahoo, Alessandro Cavalli, Alessandra A. de Souza, Erik P. A. M. Bakkers, Carlos L. Cesar, Richard Janissen,* and Monica A. Cotta*

The design and application of indium phosphide (InP) nanowire arrays to acquire *Xylella fastidiosa* bacterial cell vector force maps are discussed. The nanowire deflections are measured with subdiffraction localization confocal laser scanning microscopy (CLSM). The nanowire mechanical stability in air and liquid media as well as methods to average out thermally induced oscillations are investigated. The accuracy of center determination of the CLSM reflected laser intensity profile at nanowire apex is studied using Gaussian fitting and localization microscopy techniques. These results show that the method is reliable for measuring nanowire displacements above ≈ 25 nm. Corresponding force ranges probed by this method can be customized depending on nanowire geometry and array configuration. The method is applied to explore *X. fastidiosa* cell adhesion forces on the InP nanowire surface, and in situ probes the effect of *N*-acetylcysteine on adhered cells. Future perspectives for application of this method in microbiology studies are also outlined.

1. Introduction

Understanding microbial cell adhesion to a surface or to other cells is a fundamental step toward the full comprehension of microorganism interactions with both hosts and natural environments. This is an important research topic today due to the large impact of microbial activities in human health, biotechnology, agriculture, animal farming, industry, and economy in general.^[1–3] Quantitative measurements of cell forces are one of the approaches used to probe bacterial motility and surface interactions.^[4] However, force generation and force transmission in bacteria are less obvious than in eukaryotes; their arsenal includes a refined system to polymerize actin and acquire propulsion;^[5,6] flagellar movement, for example, induces perturbations in fluids.^[7,8] In addition, colonial

organization of bacterial cells, including the formation of biofilms, endows these organisms with a plethora of new capacities in terms of cell–cell and cell–substrate adhesion, and hence forces transmission.^[9–11] Investigations on single bacterial cell adhesion, however, can be further complicated if we consider that different surface properties, such as wettability,^[12,13] chemical constituents,^[14] compliance,^[15,16] and nanotopography,^[17–20] can influence cell behavior and adhesiveness. Moreover, environmental conditions such as pH, temperature, etc., are obviously relevant because they can affect the charge state of surface chemical groups.

Over the years, many techniques have been applied or specifically developed for measuring cell adhesion forces.^[3,21–29] Among them, flow chamber experiments have been widely used^[30,31] but they mostly capture shear forces in fluids. In the last decade, available experimental methodology was expanded by the introduction of new measurement modes based on atomic force microscopy (AFM). In single-cell force spectroscopy (SCFS), living single cells^[32,33] can be immobilized on the cantilever, thus replacing the AFM tip. This assembly is then used to probe the interaction forces to another cell or a solid substrate, and can be successfully applied to both bacteria and eukaryote investigations.^[34–38] This setup can be further improved by adding different techniques such as fluidic force microscopy technology, in which reversible bacterial cell

A. M. da Silva, Dr. P. K. Sahoo, Prof. M. A. Cotta
Applied Physics Department
Institute of Physics “Gleb Wataghin”
University of Campinas
13083-859 Campinas, São Paulo, Brazil
E-mail: monica@ifi.unicamp.br

Dr. A. Cavalli, Prof. E. P. A. M. Bakkers
Applied Physics Department
Eindhoven University of Technology
5600 MB Eindhoven, The Netherlands

Dr. A. A. de Souza
Citrus Center APTA “Sylvio Moreira”
Agronomic Institute of Campinas
13490-970 Cordeirópolis, São Paulo, Brazil

Prof. C. L. Cesar
Quantum Electronics Department
Institute of Physics “Gleb Wataghin”
University of Campinas
13083-859 Campinas, São Paulo, Brazil

Dr. R. Janissen
Kavli Institute of Nanoscience
Delft University of Technology
2629 HZ Delft, The Netherlands
E-mail: r.janissen@tudelft.nl

 The ORCID identification number(s) for the author(s) of this article can be found under <https://doi.org/10.1002/smt.201700411>.

DOI: 10.1002/smt.201700411

immobilization on the AFM tip was achieved by underpressure using a microchanneled cantilever.^[21,22] However, single point force measurements, although very valuable, cannot provide a broader picture of high data content of force networks of whole cells or multicellular tissues. Bacterial clusters and biofilms, for example, require the simultaneous measurement of forces in several anchoring points, which cannot be obtained by SCFS.

Therefore, an AFM similar concept of optically measuring a cantilever deflection to probe forces, was recently introduced using polymeric or semiconductor nanopillar arrays,^[39] capable to acquire vector force maps in parallel and real time.^[39] Several groups have demonstrated the use of force sensors based on vertical nanopillars or nanowires for mammalian cell studies.^[19,20,39–43] The use of crystalline materials with well-defined elastic properties, and stiffer than the elastomeric materials originally used for that purpose,^[19,20] improves the method accuracy. Moreover, the nanopillar aspect ratio can be varied accordingly to the force ranges of interest and the spatial distribution pattern can be fabricated to better accommodate different cell shapes and sizes, as well as their corresponding forces.

The final procedure in these arrays of force sensors is the measurement of the nanowire deflections imposed by cells adhered to the substrate. A common method has been the use of electron microscopy images^[44,45] in dry samples, with possible tension effects,^[46] which is almost impossible to apply in the case of living cells in culture. Therefore, preferable nanowire deflection optical measurements in living cells include the use of optically active semiconductor materials,^[47] or immobilizing fluorophores on the nanowire surface.^[48] In this work, we address the use of indium phosphide (InP) nanowire arrays to the map of *Xylella fastidiosa* bacterial cell adhesion forces. The deflection of nanopillars was obtained with localization subdiffraction technique in confocal laser scanning microscopy (CLSM), along with a discussion of the advantages and limitations of this technique, including an extensive study of the lower limit for the force measurement given by the precision of tip localization or the thermal limit. Furthermore, as a proof of concept for in situ, real time evaluation of cell processes, we show that this method can be used to quantitatively probe the inhibitory effect of *N*-acetylcysteine (NAC), a cysteine analog used mainly to treat human diseases, exposure on *X. fastidiosa* phytopathogenic cells which express green fluorescent protein (GFP), attached to the InP nanowires.

2. The Phytopathogenic Bacteria *X. fastidiosa* as Case Model

X. fastidiosa forms biofilms in xylem vessels in plants, causing water and nutrition stresses which affect several types of crops worldwide and causing substantial economic losses,^[49,50] and is one of the top ten phytopathogens studied in the world.^[50] Bacterial force measurements reported in literature vary significantly in range, from few piconewtons to several micronewtons in magnitude.^[21,22,24,51–54] Despite the different microorganisms used in these studies, the most likely reason for this variation is that bacterial cells employ several adhesion mechanisms;^[55,56] more importantly, if they form bacterial biofilms, adhesion proceeds through several stages, which include the cell produc-

tion of extracellular polymeric substances (EPSs), in order to make surface adhesion irreversible.^[57] Knowledge of temporal dependence of different cell adhesion mechanisms is thus important due to the expected variation in force ranges, which consequently defines the best tools for their measurement. *X. fastidiosa* biofilm formation and adhesion stages are well-documented, and have been examined at nanoscale on different biotic/abiotic surfaces^[58] as well as with single cell resolution, for bacterial strains affecting citrus plants; spatiotemporal changes in EPS composition along the bacterial life cycle were also reported.^[59] This bacterium is, therefore, one of the most suitable models for our force map investigation. More recently, *X. fastidiosa* strains started to devastate olive trees in regions of Southern Italy,^[60] and so far, no officially approved treatments are available. Instead, infected trees are usually eradicated to prevent transmission by the sharpshooters leafhoppers (*Cicadellidae*) and spittlebugs (*Cercopidae*) vectors, causing economic losses and distress among farmers.^[61] One of the few treatments currently under study is the inhibitory effect of NAC on *X. fastidiosa* biofilms. Bulk culture-based experiments and the application of NAC in infested, symptomatic sweet orange plants showed clear symptom remission and reduction in bacterial population, as analyzed by quantitative polymerase chain reaction (PCR) and bacterial isolation.^[62] Despite these interesting results, the mechanism behind the observed effects of NAC is still unknown, particularly at single cell level. We exploit here nanowire arrays to observe in situ the effect of NAC on adhered *X. fastidiosa* cells, with the objective of narrowing down possible action mechanisms and indicate potential directions of subsequent investigation of corresponding molecular mechanisms by more conventional, biological, and chemical methods.

3. Single Crystalline InP Nanowire Arrays as Cell Force Sensors

Nanowire arrays can be fabricated using different materials and processes. For applications at the biointerface, however, some requirements are imposed by the biological system under investigation. In our case, two conditions were considered. First, the geometry of the array was chosen to fit the bacterial cell dimensions. *X. fastidiosa* cells present diameters in the range 300–500 nm and lengths which can vary from 1.5 to 5 μm under normal conditions. The nanowire spatial distribution on the sample was then chosen to allow cell movement close to the surface, keeping several nanowires around each bacterial cell at any time.

A second requirement is the material system chosen for the nanowires. Semiconductor surfaces, such as Si and InP, have been shown as suitable supports for bacterial adhesion in many studies.^[39,40,58] In fact, Si nanowires have been used to demonstrate that *Shewanella oneidensis* MR-1 cells can recognize nanoscale structures; their swimming patterns and initial attachment locations are strongly influenced by the presence of nanowires on a surface.^[40] In our case, preliminary tests on flat substrates have shown that *X. fastidiosa* cells adhere and form biofilms more easily on InP substrates than on silicon or glass, among many other surfaces tested. For that reason, InP was chosen as the nanowire material for *X. fastidiosa* adhesion studies.

Regarding nanowire array fabrication, large areas are important to more easily find single cells within the limited microscope field of view. The nanowire positioning is determined by the position of the metal catalyst, usually gold, on the surface; patterning large areas can be quite time-consuming using techniques like electron beam lithography. Instead, we used nanoimprinting to create our array of Au dots.^[63]

A schematic of the fabrication method for the nanowire arrays is shown in **Figure 1A**; details can be found in the Experimental Section. Briefly, the chosen InP substrate is covered by a soft resin, such as poly(methyl methacrylate) (PMMA), and a silica-based sol-gel layer; the pattern of interest is then mechanically transferred to both materials using a Si mold.^[63] The metal layer (8 nm thick Au) is deposited prior to a lift-off procedure which removes all excess metal. In our case, 180 nm wide Au disks were patterned, with a square symmetry and a pitch of 513 nm, on a 2 in., (111)B-oriented InP wafer.^[63] The final nanowire diameter (90 nm) is defined by the amount of Au catalyst deposited.

The orientation of the substrate used here favors the formation of vertically oriented wurtzite-phase InP nanowires, with hexagonal cross-section, grown by the vapor-liquid-solid mechanism in a low pressure metalorganic vapor phase epitaxy (MOVPE) reactor. Tri-methyl-indium (TMI) and phosphine (PH₃) were used as group III and V precursors, respectively. HCl was used in situ to suppress tapering of the nanowires, which normally occurs because of vapor-solid growth on the nanowire sidewalls, unassisted by the Au particle.^[64] This procedure provides nanowires with high aspect ratio and simple-to-model mechanical behavior. Figure 1B shows scanning electron

microscopy (SEM) images of the nanowire array. We can observe that the nanowire spatial distribution is rather uniform, with approximately constant diameter along the whole nanowire length. The metal catalyst used for the growth is located at the nanowire apex. High resolution transmission electron microscopy (HRTEM) shows that the nanowires are single crystalline, wurtzite phase, as evidenced by the image in Figure 1B.

The elastic properties of nanocrystalline materials depend on the grain size and the nature of their material structure.^[65] Thus, nanowires with single crystalline phases, with none or only few structural defects, provide a good framework for force sensor applications. However, the equivalent Young's modulus (which accounts for surface effects) decreases with nanowire diameter for most materials,^[66] below ≈80 nm. Therefore, diameters at or above this value can minimize different elastic responses among nanowires due to small variations in growth. Although individual nanowire responses to mechanical perturbations can be experimentally measured^[67,68] in order to calibrate force sensitivities, this procedure unquestionably is very challenging for large areas and high nanowire densities. Considering the hexagonal nanowire as a cantilevered beam,^[69] and deflections corresponding to bending angles lower than 20° (Figure 1C), within the linear elasticity approximation, we calculate forces as^[67,70,71]

$$F = \frac{3EI}{L^3} \cdot \Delta r = \frac{15\sqrt{3}ED^4}{256L^3} \Delta r \quad (1)$$

where E depicts the Young's modulus of the nanowires, I corresponds to the second moment of inertia, D specifies

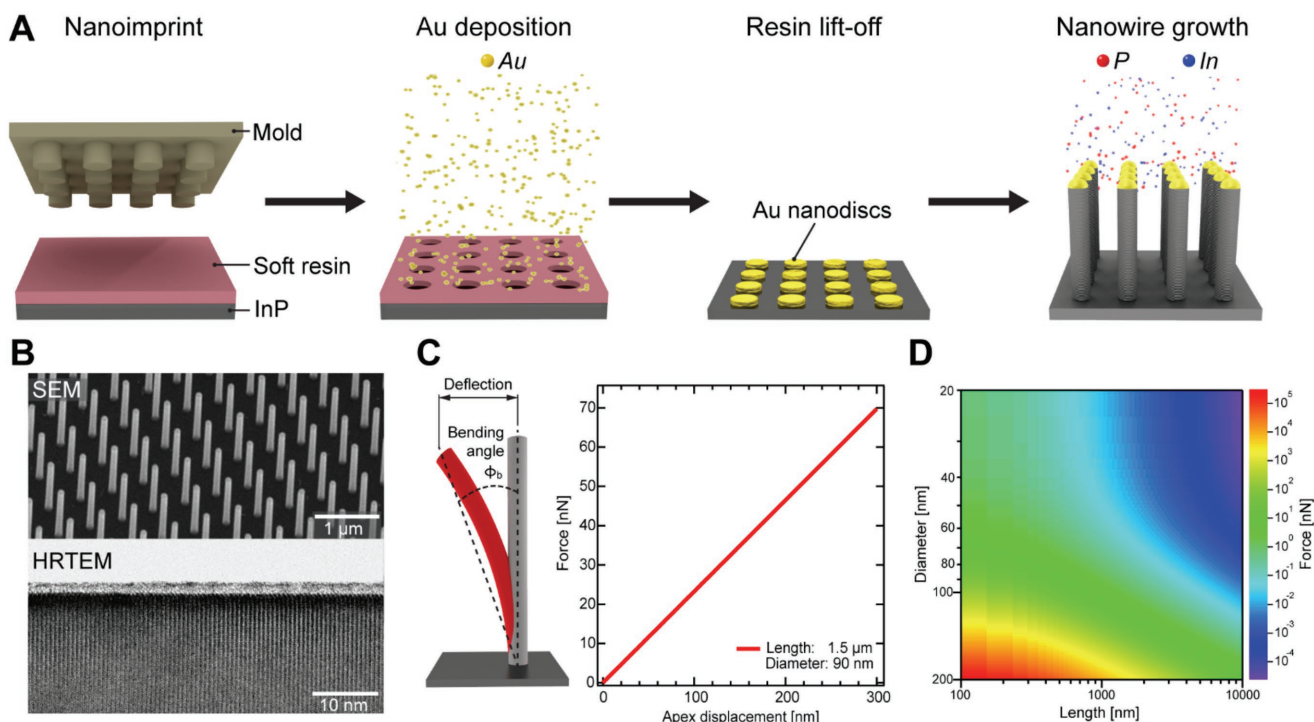


Figure 1. A) Schematic representation of nanowire growth steps using nanoimprint technique. B) SEM image, showing uniform spatial distribution of nanowires, and HRTEM image showing that the nanowires are single crystalline, wurtzite phase. C) Forces calculated as a function of apex displacements using the linear theory of elasticity for a hexagonal nanowire, with length and diameters used in this study. D) Diagram showing force ranges which can be probed by properly setting nanowire diameter and length.

the diameter of the nanowire, L identifies the length of the nanowire, and Δr determines the displacement of the nanowire apex. Considering that the positions (x, y) of the nanowire apex can be tracked along the actual trajectory, we can compute the total apex displacement as $\Delta r_i = \sqrt{(x_{i+1} - x_i)^2 + (y_{i+1} - y_i)^2}$ as well as the corresponding angle $\theta_i = \arctan\left[\frac{y_{i+1} - y_i}{x_{i+1} - x_i}\right]$. The parameters for corresponding InP nanowire arrays used in this study are: $D = 90$ nm, $L = 1500$ nm, and Young's modulus $E = 106.4$ GPa for InP (111).^[72]

Figure 1C shows that force values up to ≈ 75 nN can be measured with our nanowire dimensions, corresponding to deflections < 400 nm. However, force ranges can be varied by several orders of magnitude if both nanowire diameter and length are properly chosen, as shown in Figure 1D. The relatively straightforward fabrication process described facilitates array customization to accommodate different force ranges expected for several cell types, shapes, and dimensions. The geometry of our InP nanowire array in particular should provide a quantitative tool to study the first stages of bacterial cell adhesion, mediated by pili and EPS.^[59] Despite their importance regarding biofilm formation, these stages are not thoroughly investigated due to the lack of experimental tools.

4. Optical Measurements

In order to measure nanowire deflection caused by cell interaction, we use an optical method similar to Hallstrom et al.^[67] Basically, our InP nanowire array is loaded into a liquid cell with *X. fastidiosa* planktonic bacteria cells and Periwinkle wilt (PW) culture media,^[73] which is then measured via CLSM, in the upright configuration. The microscope focal plane (or middle of confocal volume) is confined to the region close to the top of the nanowire during force measurements (Figure 2A). As such, the confocal volume allows observation of cells attached to the nanowire apex at the same focal plane. Whenever a motile cell closely approaches or touches a nanowire, the transfer of momentum momentarily changes the nanowire deflection amplitudes. A similar, but much stronger, effect is expected for adhered cells; the configuration assumed by single cells on the surface, however, may affect the effective force range measured. This is particularly important to *X. fastidiosa* cells, for which adhesion takes place mainly through the polar region.^[59]

The bacterial strain used in our work has been modified to overexpress GFP using a genome-integrated GFP gene.^[74] The autofluorescence spectral range of bacterial cells is usually rather large. GFP allows us to reduce the spectral range, to a narrower emission band centered at 510 nm, which also facilitates differentiation of live/dead cells and possible contamination with other bacteria. GFP also provides stronger fluorescence intensity which renders cell observation easier, and allows the use of low excitation powers, for which GFP photobleaching decay times exceed several minutes. In order to excite GFP fluorescence, a 488 nm laser line is used. The laser light is also more efficiently reflected at the nanowire apex due to the presence of the metal catalyst, which shows better reflectivity than the semiconductor nanowire. The

large reflection intensity minimizes optical noise effects. It is also a factor 2–3 higher than InP luminescence in the near-infrared spectra (maximum intensity peak at ≈ 850 nm), and basically constant during measurements. Videos of bacterial cells attached or moving through nanowires, acquired simultaneously at both spectral ranges (470–498 and 507–691 nm, for nanowire apices and bacteria, respectively) are then analyzed to measure nanowire deflections associated to contact or attachment of bacteria.

In a previous report using this technique,^[39] the positions of all nanowire tips in a video frame were tracked by considering them as solid circular particles (Figure 2B); the center of the circle was computed from the position of horizontal and vertical Feret diameters of a circular post. This procedure was automatically carried out after appropriately choosing the region of interest in the particle analysis plugin of ImageJ/Fiji.^[75] The background noise in the measurement was obtained by means of tracking an isolated control nanowire, not associated with a bacterial cell, in the same image field of view. The results obtained for nanowires attached with *X. fastidiosa* cells show measured displacements usually larger than those for the control case. However, small displacements (corresponding to forces lower than ≈ 5 nN) composed the larger part of the measurements, and could be attributed to mechanical noises in the setup. Here, we show the complete analysis procedure of the measurements in order to understand the origin of this noise and extract accurate force values within the resolution of our setup.

The lower limit for the force measurement comes from the precision of the measurement of the apex position of each nanowire. A naïve estimation would just use theoretical limits of a confocal microscopy and assume that a minimum measurable deflection is ≈ 200 nm, or 0.13 radians ($\approx 7.5^\circ$) for a 1500 nm long nanowire. More strictly, as we only have to measure the deflection in one direction, we should use ≈ 100 nm, or 0.07 radians ($\approx 3.8^\circ$), as the lower limit. However, we can compare our system with super-resolution localization microscopy. Localization microscopy must ensure that no two molecules emit inside the diffraction spot size, what can be achieved by, e.g., turning on and off the molecules emission. Indeed, using super-resolution techniques, traction force microscopy spatial resolution and accuracy of force reconstruction have been significantly improved.^[27,28] In our case, each nanowire is more than a diffraction spot size apart, so we do not encounter this problem. Moreover, the precision of the localization method goes with the square root of the number of photons detected. In our case, the laser reflection on the nanowire apex is about one order of magnitude larger than the typical number of emitted fluorescent photons. The resolution of confocal microscopy involves two diffraction widths: the spot size of the excitation beam, and the collected emission beam. In the present case, the reflection comes from the ≈ 90 nm nanowire apex, much smaller than the ≈ 400 nm spot size of the excitation laser beam. So, the light source can be considered a point source from the excitation point of view. Moreover, any instrument drift during the experiment can be corrected by the position of several control nanowires within a field of view with a much better resolution than by individual nanowire localization. Although the theory for a single dipole emitter in ideal situation leads to an Airy function, it has been observed that a Gaussian curve better fits the data.^[76]

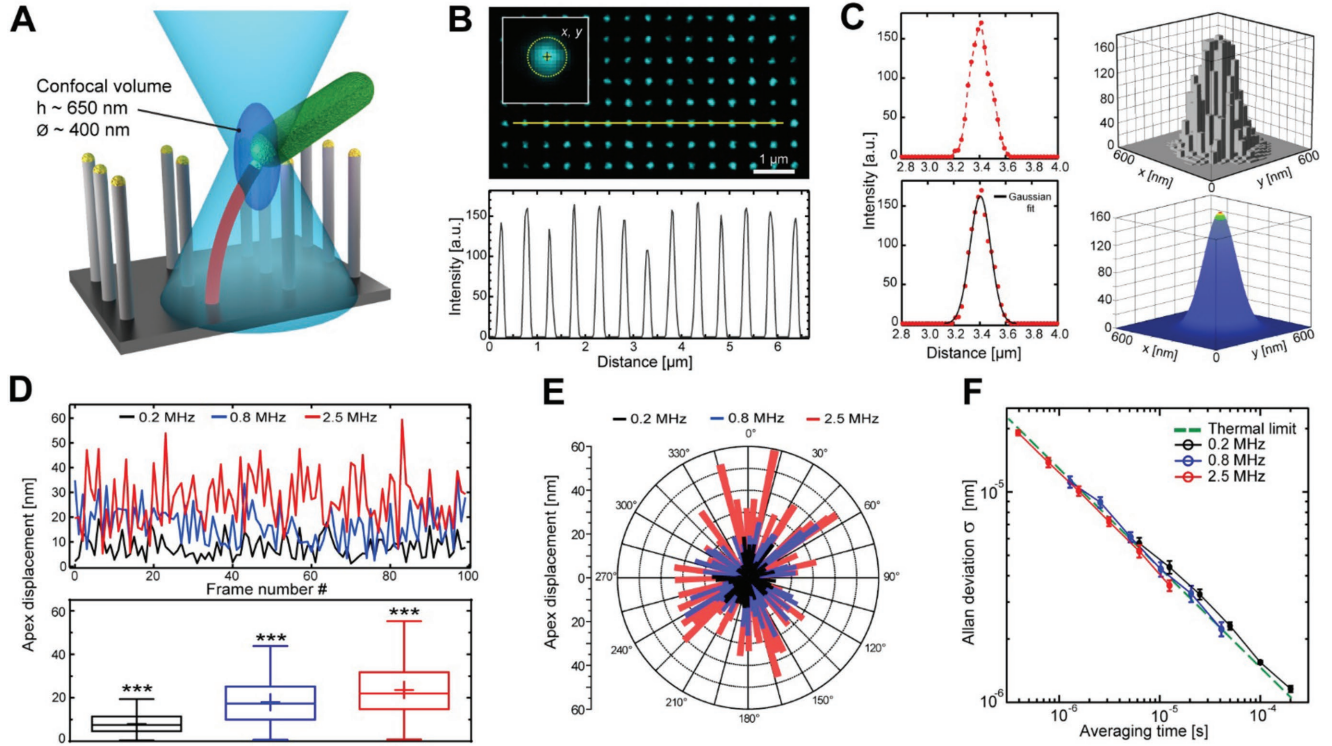


Figure 2. A) Schematic representation of nanowire array with single bacterium attached showing that the confocal volume, defined by the optical configuration, allows the simultaneous observation of bacteria pole and nanowire apex at the same focal plane. B) CLSM image of nanowire array, with dots representing the laser intensity reflected at the nanowire apex. The inset shows the intensity pattern for a single nanowire. C) 1D and 2D experimental intensity profiles (top) and corresponding Gaussian fit (bottom) for both the cases. D) Apex displacements values, obtained from center localization using Gaussian fitting for sequential video frames, for measurements with different pixel net frequencies (0.2, 0.8, and 2.5 MHz). Tukey box plot shows significant differences for the three measurement conditions. E) Polar plot provides displacement magnitudes and bearings. F) Allan deviation plot exhibits that the thermal limit is reached for the three measurement cases. One-way analysis of variance (ANOVA) and comparison via Tukey post hoc test with $p = 0.0001$ were carried out for statistical analysis.

Therefore, we decide to calculate displacements using a Gaussian fitting of nanowire apex deflections instead of Feret diameters.^[39] We can observe from Figure 2B,C that indeed the Gaussian function properly describes our data, providing the center, linewidth, and height of the reflection pattern. For the 1D case, the residual sum of squares (RSS) associated to the fitting can be written as

$$\chi^2(\vec{\alpha}_j) = \sum_i [y_{\text{exp}}(x_i) - y_{\text{fit}}(x_i; \vec{\alpha}_j)]^2 \quad (2)$$

where $\vec{\alpha}_j$ are the nonlinear parameter vectors for each function $f_j(x)$, so that

$$y(x) = \sum_j A_j f_j(x; \vec{\alpha}_j) \quad (3)$$

In order to estimate the resolution of our technique, we extracted from the observation data how precisely we can determine the center of a Gaussian for each nanowire. For that, we consider the nonlinear parameters that minimize the RSS, so that

$$\chi^{2*} = \chi^2(\vec{\alpha}_j^*) = \text{Min}[\chi^2(\vec{\alpha}_j)] \quad (4)$$

and the total variance of the curve

$$\sigma^{2*} = \frac{1}{n} \chi^{2*} \quad (5)$$

where n is the number of experimental points observed. Once the minimum RSS and the curve variance are found, we assume a normal distribution for χ^2 such as

$$f(\chi^2) = A e^{-\frac{\chi^2}{2\sigma^2}} \quad (6)$$

and search one nonlinear parameter at a time, keeping all the other parameters fixed, for which

$$\frac{\chi^2(\alpha_i^* + \delta\alpha_i) - \chi^2(\alpha_i^*)}{\sigma^2} - 1 = 0 \quad (7)$$

for each side of the curve, that is, $\delta\alpha_i > 0$ and $\delta\alpha_i < 0$. With that procedure, we obtained the precision range for the i th parameter $\alpha_i \in [\alpha_i^* - \delta\alpha_i^-, \alpha_i^* + \delta\alpha_i^+]$, where $\delta\alpha_i^\pm = |\delta\alpha_i|$. Any simulation generating random residuals around a Gaussian curve will show that we are capable to discriminate between two curves whose parameters are out of this precision range.

We have then used this methodology to find the precision intervals for the center of the experimental reflection patterns, considered as 2D Gaussian curves (Figure 2C), which represent the nanowire apex position. In general, we obtain $2 \text{ nm} < (\delta\alpha_i^*)_{x,y} < 6 \text{ nm}$, depending on scan speed, for control nanowires observed in PW media. We can then assume that it is possible to discriminate, by Gaussian fitting, two patterns with centers displaced by more than 5 nm. This sets the lower limit of 0.003 radians (0.17°) for nanowire displacement precision. Figure 2C illustrates the 1D and 2D data points and the corresponding Gaussian fittings. In the latter case, the spatial delocalization of the nanowire apex is shown by the graded colored region superimposed on the blue 2D Gaussian curve. This analysis provides good support to the use of Gaussian fitting for these experiments. The motion of control nanowires with time in PW media was then analyzed by fitting several nanowire reflection patterns with 2D Gaussian functions, in frames extracted from the CLSM video files. The images were acquired with three different pixel net scan speeds, from 0.5 to 8 Hz. Considering 512×512 pixels in the image, we calculate pixel dwell times of 0.4, 1.3, and $6.3 \mu\text{s}$ (and corresponding pixel net frequencies of 2.5, 0.8, and 0.2 MHz, respectively). Figure 2D shows nanowire apex displacements calculated using the center position of the fitted Gaussian curves in each case.

Nanowires cantilevered to a substrate are free to vibrate at the tip. Resonance can be excited thermally, with the free end oscillating with an amplitude that depends on temperature as well as nanowire composition and geometry, which determine its stiffness.^[69,77] Considering the calculated spring constant of $\approx 0.2 \text{ N m}^{-1}$ of our nanowires,^[39] a resonance frequency in air of $\approx 10 \text{ MHz}$ can be estimated. This value drops by a factor 3–5 for oscillations in liquid environment;^[78] as we increase the scan speed, we probe the position of each nanowire in the image with smaller pixel dwell times; larger amplitudes are then observed in our data ensemble (Figure 2D). On the other hand, larger pixel dwell times entitle a larger time average of the nanowire position, yielding smaller amplitudes, as shown in Figure 2D. In fact, statistically significant differences in nanowire apex displacements are observed as we increase the pixel net frequency. A comparison of the same data evaluated using Feret diameters does not allow discrimination of the data sets at larger speeds.

The oscillations associated with those displacements are isotropic in spatial nature, as expected from thermal excitation. The Allan deviation plot (Figure 2F) illustrates that this is indeed the case.^[79,80] A similar behavior can be observed for nanowire oscillations probed by CLSM in air. Spatially isotropic amplitudes increase with scan speeds, as shown in Figure S1A,B (Supporting Information), and the Allan deviation affirms the behavior expected from thermal excitation (Figure S1C, Supporting Information). The nanowire amplitudes are larger than in liquid (PW), as expected from lower energy dissipation from hydrodynamic forces acting opposite to the nanowire movement direction, and the resulting higher quality factors for oscillations in air. However, the statistics shown in the box plot (Figure S1D, Supporting Information) suggest that the time averaging of nanowire position provided by measurements using lower pixel net frequencies results in indistinguishable data sets. Once chosen the geometry of the

nanowire arrays, it is thus very likely that thermal oscillations impose the lower limit for averaged displacements at around 20–25 nm,^[39] which lies within the resolution of our observation technique in liquid media, as discussed above. This result imposes a lower limit for force measurements using our nanowire arrays at $\approx 4\text{--}5 \text{ nN}$. Regarding bacterial adhesion processes, this limit prevents the application of our method to pili-mediated cell adhesion, for example, since protein–surface interactions would provide forces in the range of tens or hundreds of piconewtons.^[58,81]

5. Probing the Effect of NAC on Nanowire-Adhered Bacteria

In order to show one of the possible applications of nanowire arrays, we evaluate in real time the effect of NAC on *X. fastidiosa* single cells attached to individual nanowires. As shown in previous studies,^[39,59] adhesion can take place in different configurations, with *X. fastidiosa* cells oriented vertically or horizontally to the surface (Figure 3A). The scanning electron microscopy image of a sample with 24 h culture time illustrates cell binding to the neighboring nanowires, and their corresponding deflections. After a few hours of culture time, adhesion takes place via EPS deposition,^[59] which is not easily observed in CLSM images. In particular, for our ex vivo experiments, cells were grown in the liquid cell for 12 h, which translates into a lower EPS-secreted volume and cell polar regions more firmly attached than the body. CLSM images were first used to observe the amount of cells and their spatial distribution in the sample. Once cell density was adequate and nanowire-adhered bacteria were found, we added NAC (2 mg mL^{-1}) to the liquid cell and subsequently observed single cells for several minutes (up to 30 min, for each chosen cell or cell cluster). The NAC concentration was chosen based on values from previous in vitro studies.^[62] The displacements of nanowires attached to the cells were measured over time, as well as control nanowires in the same field of view. No significant photobleaching of the cell GFP was observed within these time frames and the laser power chosen. Most cells observed under NAC exposure were eventually released from the nanowires, as schematically shown in Figure 3B (see also Video S1 in the Supporting Information). This behavior was not observed in cell cultures, with similar growth and observation times, which were not exposed to NAC (Video S2, Supporting Information).

We analyze in more detail the temporal dependence of adhesion force for a motile bacterial cell, horizontally attached to a single nanowire. The plot in Figure 3B shows that tracking adhesion forces makes possible to pinpoint the moment when the cell loses contact with the nanowire, after $\approx 86 \text{ min}$ of NAC addition to the liquid cell that holds the sample. Moreover, average forces before and after that moment are different. In fact, slightly larger forces are observed just before the release of the cell, most likely due to the larger degree of freedom for cell motion in this case.

Figure 3C shows the statistical distribution of adhesion forces calculated from the measured nanowire displacements. We can observe that the force values for the bound nanowire compare well with those expected from previously reported results;^[39] upon release of the cell, the formerly bound nanowire (“free” in

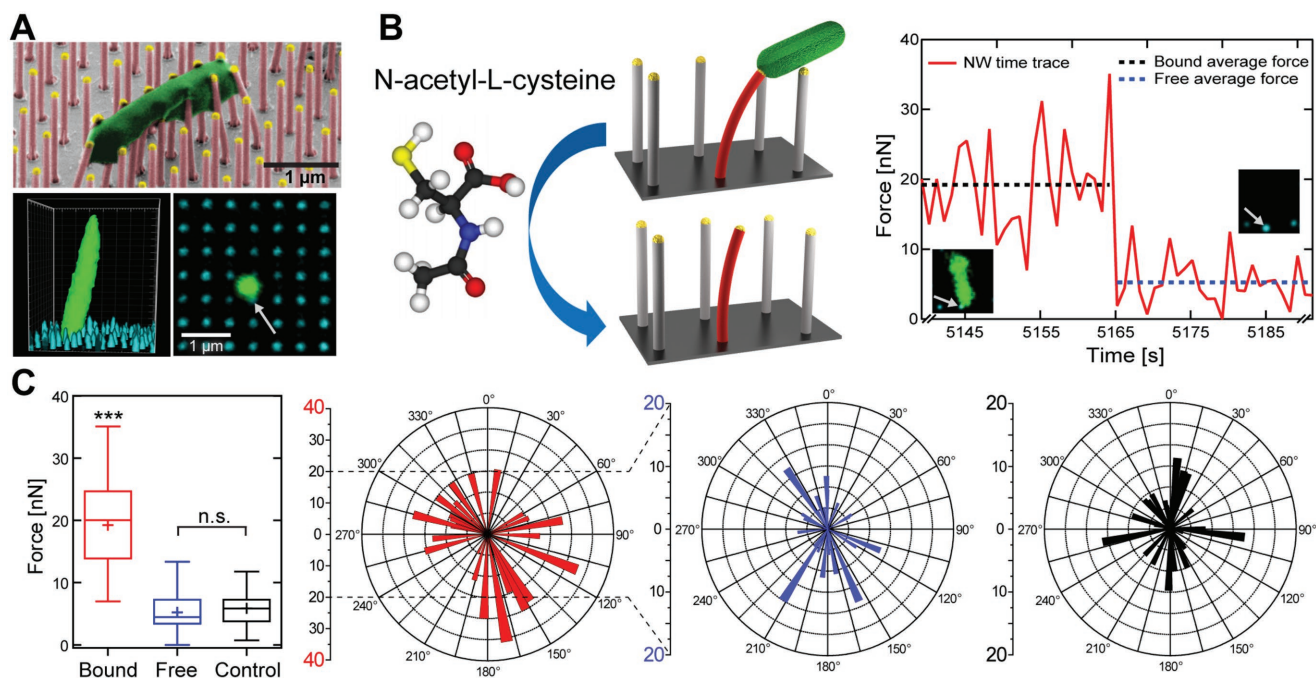


Figure 3. A) Color-enhanced SEM image illustrating a bacterial cell horizontally adhered to the nanowires after 24 h growth time, and CLSM images showing a 3D rendering of a vertically adhered bacterial cell and a single plane with the polar region of the bacteria attached to a nanowire, indicated by the white arrow. B) Schematic representation illustrating bacterial releasing from the nanowire due to NAC action (left) and temporal force plot before and after bacteria release (right); the white arrows at the inset images indicate the nanowire where bacteria was attached. C) Tukey box plot showing force value distributions calculated for the nanowire where the bacteria was attached (bound), after bacteria release (free), and for a control nanowire in the same image without any bacteria. Polar plots depict the magnitudes and bearings of the corresponding forces. One-way ANOVA and comparison via Tukey post hoc test with $p = 0.0001$ were carried out for statistical analysis.

Figure 3C) shows significantly lower forces, no longer distinct from thermally driven oscillating, control nanowires. The polar plot for the adhesion forces presents smaller forces (up to ≈ 10 nN) with isotropic angular distribution for the free as well as for control nanowires. The bound nanowire, on the other hand, exhibits in average fourfold larger forces (≈ 20 – 40 nN) distributed across the whole angular region; however, a few, stronger force values are observed at angular values opposed to that occupied by the cell (typical angular orientation of the cell is shown in the fluorescence image inset of Figure 3B).

Several mechanisms are proposed in literature as possible causes for the NAC effect. Among them,^[82] sulfhydryl groups in NAC are considered to possibly disrupt disulfide bonds of bacterial enzymes involved in EPS production or secretion through thiol–disulfide exchange. In the particular case of *X. fastidiosa*, Muranaka et al.^[62] speculate that NAC could avoid the formation of disulfide bonds involved in attachment and aggregation via adhesion proteins containing cysteine residues. One of the effects reported by these authors is the inability of cells to adhere and form biofilm; a significant increase in planktonic biomass was found, with the fraction of viable cells depending on NAC concentrations used.^[62] For different bacteria, however, some authors found no detectable degradation of EPS by NAC and thus suggested that NAC reduced the production of EPS.^[83] More recently, Picchi et al. study on *Xanthomonas citri*^[84] showed that, although the total amount of EPS did not differ among the treatments, a dose-dependent response was observed for the relative amounts of EPS in the

pellet and supernatant with different NAC concentrations, with a reduction in the EPS in the pellet as NAC increased.

Although preliminary, our results using nanowires as real time force sensors can contribute to this ongoing discussion about antimicrobial effects of NAC down to the scale of single cells. We show the abrupt release of *X. fastidiosa* cells already adhered to a single nanowire, upon NAC exposure for several minutes at concentrations that affect adhesion, biofilm formation, and EPS production, according to in vitro studies.^[62] The growth times used in our study provided EPS-mediated adhesion of *X. fastidiosa* cells, particularly at cell poles,^[59] and cell release was observed for relatively short time periods – as compared to those required for changes in gene expression – after NAC addition. Our data thus suggest EPS dissolution as one of the mechanisms for transferring cells from sessile to planktonic states. Indeed, in our experiments, not all cells were released within the time frame of observation, as expected if EPS coating thickness variation occurs. It is also feasible to assume that dissolution of EPS depends on its composition. Soluble EPS, which is the first to be secreted by the bacteria,^[59] is most likely the easiest to be removed since it can be dissolved rather easily in the surrounding media.

On the other hand, the semifloating nature of *X. fastidiosa* biofilms may also facilitate their transfer to the planktonic state. Reasonably large bacterial clusters and mature biofilms are anchored to the surface by only a few cells;^[59] if these cells can be detached as observed here for single vertical cells, the whole cluster will separate from the surface and may not reattach.

Indeed, in one of our experiments, we have observed such behavior (Video S3, Supporting Information).

6. Discussion

One of the bottlenecks for studying mature biofilms with nanowire arrays such as ours is the increasing biomass (cells and EPS) as growth proceeds. In particular, EPS contains many types of biomolecules, such as lipids, DNA, proteins, and polysaccharides.^[57] Moreover, EPS composition changes over time, along the bacterial life cycle.^[59] The larger biomass translates into larger absorption and scattering rates for the excitation laser along the optical path. Thus, attenuated intensities for the laser reflection at nanowire apex are expected. This is indeed the case when larger clusters and biofilms are present on the surface; nanowires are not entirely visible during the time window of the experiment (Video S3, Supporting Information).

Using fluorophores to decorate the nanowires is one of the possible options present in literature,^[47,67] however, in this case, the excitation intensity is attenuated as well and fluorescence emission will be proportionately weaker, particularly if absorption at this spectral range takes place. Moreover, eventual photobleaching cannot be prevented for extended observation times. An alternative to minimize this problem was developed by Li et al.^[85] by inserting an InGaP quantum dot in the GaP nanowire. The quantum dot emits in the visible range, while the nanowire matrix, with indirect bandgap, does not show photoluminescence. Despite the need for enough optical excitation power in order to create electron–hole pairs in the semiconductor material forming the quantum dot, it is possible to tune the whole system so that the photoluminescence lies within optical windows in the system.

Nanowire arrays can also be functionalized with surface coatings to explore adhesion under different chemical environments. This is particularly interesting for species such as *X. fastidiosa*, which inhabits different hosts, xylem plants, and the foregut of the vector insect. These two environments are chemically distinct, with cellulose and chitin as their primary surface components, respectively. Adhesiveness modulation is used by this bacterium in order to colonize the plant xylem and transfer cells between different hosts.^[86] Functionalized nanowire arrays can be an effective tool to quantitatively study this mechanism in situ, as already shown in the case that adhesins were immobilized at the nanowire surface.^[39] However, absolute force measurements for cell clusters and biofilms may be more difficult to probe due to the possible mechanical influence of EPS matrix.^[31] The presence of larger EPS volumes may dampen nanowire motion in such a way that their deflections eventually become nonrepresentative of the applied individual forces.

On the other hand, the presence of the arrays is not strictly necessary for sensing applications. Instead, nanowires in large densities can be used^[40] so as to maximize the probability of cell adhesion – and easily finding a bacterial cell on the surface at the higher magnifications necessary for improved nanowire apex localization. However, nanowire arrays can be tailored to customize the problem at hand, for example, guiding cell movement or assembly, as shown in previous works,^[19,39] while simultaneously providing force measurements.

7. Conclusion

We have shown here the use of nanowire arrays as force sensors for bacterial adhesion. *X. fastidiosa* cells expressing GFP were grown on InP nanowire vertical arrays and observed with CLSM. Bacterial cells were identified by GFP fluorescence; the reflected laser intensity at the nanowire apex was used to track its position along time, providing nanowire deflections related to the presence of the adhered bacteria. Adhesion forces were then calculated from the deflection data using linear elasticity theory. In order to validate our method, we characterize the nanowire motion in air and liquid as a function of CLSM scan speed, and show that thermally induced oscillations can be average out. The center of the nanowire intensity profile was calculated using 2D Gaussian fitting; the uncertainty of this position was estimated as lower than 6 nm using a localization microscopy concept. These results altogether show that our method is reliable for measuring nanowire displacements above ≈ 25 nm, or force values larger than ≈ 5 nN for our nanowire geometry. Our force sensor was then used for the first time to track in situ and in real time the abrupt cell release under the effect of *N*-acetylcysteine, which shows an inhibitory effect on *X. fastidiosa* biofilms as well as in many different Gram negative and Gram positive bacteria. Our observation suggests EPS dissolution as a possible mechanism for cell transfer from sessile to planktonic states.

8. Experimental Section

Indium Phosphide Nanowire Array Growth: Nanowires were grown in a low-pressure Aixtron Closed Coupled Showerhead (CCS) MOVPE machine, using hydrogen (H_2) as precursor carrier gas. The total flow was 6 L min^{-1} at a pressure of 50 mbar. The vapor–liquid–solid (VLS) method, in which Au droplets act as catalysts, was used to grow the nanowires on (111)-oriented InP substrates. For that reason, 8 nm thick, 180 nm wide Au disks were patterned, with a square symmetry and a pitch of 513 nm, by nanoimprint lithography on a 2 in. wafer.^[63] Before nanowire growth, an annealing step at 510 °C under PH_3/H_2 atmosphere was performed to remove organic residues from the nanoimprint process. TMI and PH_3 were used as group III and V precursors. p-doped nanowires were obtained by doping in situ by diethyl-zinc (DEZn) with a molar fraction of 6×10^{-6} . A constant molar fraction of HCl was used in situ during growth in order to suppress tapering of the nanowires.^[64] Growth times of p-doped nanowires were 18 min, after a short 1 min undoped stem.^[87] Nanowires grew vertically, perpendicular to the substrate, in the $\langle 111 \rangle$ direction. The typical diameter and length of the nanowires in the array were 90 and 1500 nm, respectively. For bacterial adhesion studies, the substrates were cut into rectangular pieces of $\approx 2 \times 3$ mm.

Substrate Materials and Cleaning Process: For all bacterial adhesion experiments carried out in this work, InP nanowire arrays were cleaned to remove inorganic as well as organic contamination, and sterilized in a final step. To do so, the substrates were cleaned with acetone, isopropanol, and deionized water, and dried with a gentle nitrogen flow. The substrates were sterilized by oxygen plasma (SE80, Barrel Asher Plasma Technology, USA) for 15 min (50 sccm O_2 , 100 W, 100 mTorr) immediately prior to the experiment.

Bacteria Strains: *X. fastidiosa* GFP expressing strain 11399 was used in this study. PW broth media^[73] with bovine serum albumin (BSA) was used as bacterial growth media.

Bacteria Extraction and Inoculum Preparation: The extraction and growth of *X. fastidiosa* strains from citrus-variegated chlorosis (CVC) symptomatic sweet orange trees were described previously.^[59,88] Briefly, harvested cells were resuspended in phosphate-buffered saline (PBS)

(pH 7.4) buffer and the concentration was adjusted to optical density (OD)₆₀₀ = 0.3. Afterward, the strains were grown in PW broth and incubated at 28 °C for 7 days in a rotary shaker at 180 rpm.

CLSM Imaging of InP Nanowire Arrays without Bacterial Cells: InP nanowire arrays were placed inside a Teflon dish (10 mm diameter and 5 mm in height). Then, 400 µL of PW broth media, without bacterial cells, was injected inside the Teflon dish, which was covered with a sterilized borosilicate cover glass with ≈0.16 mm of thickness. Recording of nanowire tip positions were performed using CLSM system [Zeiss LSM780-NLO confocal microscope (Carl Zeiss AG, Germany)] with a 40× water-immersion objective (W Plan-Apochromat, numerical aperture (NA) 1.0). A 488 nm laser line and the tip position of each nanowire were identified by the reflected laser. The pinhole diameter and gain were adjusted as the scan speed was changed, in order to get a better signal–noise ratio. Videos were recorded by acquiring 100 frames in time series measurements for three different pixel net scan speeds: 0.2, 0.8, and 2.5 MHz.

CLSM Ex Vivo Imaging of *X. fastidiosa* on InP Nanowire Arrays and NAC Experiments: GFP expressing *X. fastidiosa* strain 11399^[74] were used in this study. Bacterial inoculum in PW broth media with a concentration of 1 × 10⁷ colony-forming unit (CFU) mL⁻¹ were used for the ex vivo adhesion experiments. InP nanowire arrays (sample dimensions ≈ 2 × 3 mm²) were placed inside a custom made Teflon dish (10 mm diameter and 5 mm in height). 400 µL of inoculum was injected inside the Teflon dish and subsequently covered with a sterilized borosilicate cover glass. The assembly was further incubated inside a bacterial oven (410/3NDR, Nova Ética, Brazil) at 28 °C for 12 h prior to the ex vivo CLSM measurements. Simultaneous recording of bacteria and nanowire location were performed using CLSM system [Zeiss LSM780-NLO confocal microscope (Carl Zeiss AG, Germany)] with a 100× oil-immersion objective (Plan-Fluar, NA 1.45). Using a 488 nm laser excitation, the temporal positions of nanowire and bacteria cells were simultaneously measured in two different channels. Directly reflected laser line was used to locate the position of the individual nanowires, while wavelength channel width of 507–691 nm (fluorescence emission of GFP) was used to collect the position of bacteria. A specific concentration of NAC 2.0 mg mL⁻¹ was added to the Teflon dish (liquid cell), and few bacteria motion, attached to nanowire, were tracked over time, almost immediately after NAC addition, for several minutes. All images were recorded with a pinhole of ≤1 Airy unit for each channel with 512 × 512 px (nanowire with bacteria) and distances of 370 nm for the z-stack. The 3D-stacked images were analyzed with ImageJ/Fiji for video extraction and particle analysis by Feret diameters; center coordinates were extracted for each nanowire of interest in all video frames. Specific routines were written in Python for the 2D Gaussian fitting and apex position uncertainty analysis.

Supporting Information

Supporting Information is available from the Wiley Online Library or from the author.

Acknowledgements

The authors acknowledge J. H. Clerici, V. B. Pelegati, and M. O. Baratti for technical assistance, and Prof. H. F. de Carvalho and Prof. A. A. de Thomaz, from the University of Campinas, for valuable discussions. A.C. and E.P.A.M.B. would like to acknowledge Rene Van Veldhoven for the exceptional work and care for the MOVPE systems, and the technical support from the NanoLab@TU/e cleanroom. This work was financially supported by the FAPESP (Fundação de Amparo a Pesquisa do Estado de São Paulo, Brazil), through grants 2010/51748-7, 2013/02300-1, and 2013/10957-0 and the CNPq (Conselho Nacional de Desenvolvimento Científico e Tecnológico, Brazil), grant number 479486/2012-3. A.M.d.S. acknowledges scholarship from the CNPq; P.K.S. acknowledges the FAPESP for funding his scholarship. M.A.C., A.A.d.S., and C.L.C. acknowledge the CNPq research fellowships. The

authors thank the access to confocal microscopy equipment provided by the National Institute of Science and Technology on Photonics Applied to Cell Biology (INFABIC) at the University of Campinas; INFABIC is cofunded by the FAPESP (08/57906-3) and the CNPq (573913/2008-0). The authors also acknowledge the National Nanotechnology Laboratory (LNNano) at the CNPEM, Brazil, for granting access to their electron microscopy facilities. A.C. and E.P.A.M.B. acknowledge the funding of the Dutch Technology Foundation STW (Project 11826), which is part of the Netherlands Organisation for Scientific Research (NWO), and which is partly funded by the Dutch Ministry of Economic Affairs.

Conflict of Interest

The authors declare no conflict of interest.

Keywords

biofilms, cell adhesion forces, confocal microscopy, nanowires, *Xylella fastidiosa*

Received: December 20, 2017

Revised: April 12, 2018

Published online:

- [1] L. Hall-Stoodley, J. W. Costerton, P. Stoodley, *Nat. Rev. Microbiol.* **2004**, *2*, 95.
- [2] T. Danhorn, C. Fuqua, *Annu. Rev. Microbiol.* **2007**, *61*, 401.
- [3] T. R. Garrett, M. Bhakoo, Z. Zhang, *Prog. Nat. Sci.* **2008**, *18*, 1049.
- [4] W. J. Polacheck, C. S. Chen, *Nat. Methods* **2016**, *13*, 415.
- [5] M. D. Welch, A. Iwamatsu, T. J. Mitchison, *Nature* **1997**, *385*, 265.
- [6] V. Benza, *Phys. Biol.* **2008**, *5*, 26002.
- [7] M. J. Tipping, N. J. Delalez, R. Lim, *mBio* **2013**, *4*, e00551.
- [8] H. C. Berg, *Annu. Rev. Biochem.* **2003**, *72*, 19.
- [9] J. W. Costerton, *Science* **1999**, *284*, 1318.
- [10] A. Rajasekar, B. Anandkumar, S. Maruthamuthu, Y. P. Ting, P. K. S. M. Rahman, *Appl. Microbiol. Biotechnol.* **2010**, *85*, 1175.
- [11] P. C. Bogino, M. de las Mercedes Oliva, F. G. Sorroche, W. Giordano, *Int. J. Mol. Sci.* **2013**, *14*, 15838.
- [12] G. M. Bruinsma, H. C. van der Mei, H. J. Busscher, *Biomaterials* **2001**, *22*, 3217.
- [13] Y. Liu, Q. Zhao, *Biophys. Chem.* **2005**, *117*, 39.
- [14] A. Pranzetti, S. Mieszkin, P. Iqbal, F. J. Rawson, M. E. Callow, J. A. Callow, P. Koelsch, J. A. Preece, P. M. Mendes, *Adv. Mater.* **2013**, *25*, 2181.
- [15] N. Saha, C. Monge, V. Dulong, C. Picart, K. Glinel, *Biomacromolecules* **2013**, *14*, 520.
- [16] J. A. Lichter, M. T. Thompson, M. Delgado, T. Nishikawa, M. F. Rubner, K. J. Van Vliet, *Biomacromolecules* **2008**, *9*, 1571.
- [17] R. J. Crawford, H. K. Webb, V. K. Truong, J. Hasan, E. P. Ivanova, *Adv. Colloid Interface Sci.* **2012**, *179–182*, 142.
- [18] L. Rizzello, B. Sorce, S. Sabella, G. Vecchio, A. Galeone, V. Brunetti, R. Cingolani, P. P. Pompa, *ACS Nano* **2011**, *5*, 1865.
- [19] A. I. Hochbaum, J. Aizenberg, *Nano Lett.* **2010**, *10*, 3717.
- [20] P. Kim, A. K. Epstein, M. Khan, L. D. Zarzar, D. J. Lipomi, G. M. Whitesides, J. Aizenberg, *Nano Lett.* **2012**, *12*, 527.
- [21] E. Potthoff, D. Ossola, T. Zambelli, J. A. Vorholt, *Nanoscale* **2015**, *7*, 4070.
- [22] O. Guillaume-Gentil, E. Potthoff, D. Ossola, C. M. Franz, T. Zambelli, J. A. Vorholt, *Trends Biotechnol.* **2014**, *32*, 381.
- [23] O. Axner, M. Andersson, O. Björnham, M. Castelain, J. Klinth, E. Koutris, S. Schedin, in *Bacterial Adhesion: Chemistry, Biology and Physics* (Eds: D. Linke, A. Goldman), Advances in Experimental Medicine and Biology, Springer, Dordrecht **2011**, pp. 301–313.

- [24] E. Fällman, S. Schedin, J. Jass, M. Andersson, B. E. Uhlin, O. Axner, *Biosens. Bioelectron.* **2004**, *19*, 1429.
- [25] O. Galy, P. Latour-Lambert, K. Zrelli, J. M. Ghigo, C. Beloin, N. Henry, *Biophys. J.* **2012**, *103*, 1400.
- [26] N. Walter, C. Selhuber, H. Kessler, J. P. Spatz, *Nano Lett.* **2006**, *6*, 398.
- [27] H. Colin-York, D. Shrestha, J. H. Felce, D. Waithe, E. Moeendarbary, S. J. Davis, C. Eggeling, M. Fritzsche, *Nano Lett.* **2016**, *16*, 2633.
- [28] H. Colin-York, C. Eggeling, M. Fritzsche, *Nat. Protoc.* **2017**, *12*, 783.
- [29] Q. Huang, J. Lee, F. T. Arce, I. Yoon, P. Angsantikul, J. Liu, Y. Shi, J. Villanueva, S. Thamphiwatana, X. Ma, L. Zhang, S. Chen, R. Lal, D. J. Sirbuly, *Nat. Photonics* **2017**, *11*, 352.
- [30] H. J. Busscher, H. C. Van Der Mei, *Clin. Microbiol. Rev.* **2006**, *19*, 127.
- [31] M. P. Monteiro, J. H. Clerici, P. K. Sahoo, C. L. Cesar, A. A. de Souza, M. A. Cotta, *Colloids Surf., B* **2017**, *159*, 174.
- [32] A. Beaussart, S. El-Kirat-Chatel, R. M. A. Sullan, D. Alsteens, P. Herman, S. Derclay, Y. F. Dufrêne, *Nat. Protoc.* **2014**, *9*, 1049.
- [33] D. Martínez-Martín, G. Fläschner, B. Gaub, S. Martin, R. Newton, C. Beerli, J. Mercer, C. Gerber, D. J. Müller, *Nature* **2017**, *550*, 500.
- [34] M. Benoit, D. Gabriel, G. Gerisch, H. E. Gaub, *Nat. Cell Biol.* **2000**, *2*, 313.
- [35] E. P. Wojcikiewicz, *J. Cell Sci.* **2003**, *116*, 2531.
- [36] P.-H. Puech, *J. Cell Sci.* **2005**, *118*, 4199.
- [37] J. Helenius, C.-P. Heisenberg, H. E. Gaub, D. J. Muller, *J. Cell Sci.* **2008**, *121*, 1785.
- [38] Y. F. Dufrêne, *Trends Microbiol.* **2015**, *23*, 376.
- [39] P. K. Sahoo, R. Janissen, M. P. Monteiro, A. Cavalli, D. M. Murillo, M. V. Merfa, C. L. Cesar, H. F. Carvalho, A. A. De Souza, E. P. A. M. Bakkers, M. A. Cotta, *Nano Lett.* **2016**, *16*, 4656.
- [40] H. E. Jeong, I. Kim, P. Karam, H. J. Choi, P. Yang, *Nano Lett.* **2013**, *13*, 2864.
- [41] K. K. Sakimoto, C. Liu, J. Lim, P. Yang, *Nano Lett.* **2014**, *14*, 5471.
- [42] L. Wang, H. Wang, L. Yuan, W. Yang, Z. Wu, H. Chen, *J. Mater. Chem.* **2011**, *21*, 13920.
- [43] H. Wang, L. Wang, P. Zhang, L. Yuan, Q. Yu, H. Chen, *Colloids Surf., B* **2011**, *83*, 355.
- [44] Z. Li, J. Song, G. Mantini, M. Y. Lu, H. Fang, C. Falconi, L. J. Chen, Z. L. Wang, *Nano Lett.* **2009**, *9*, 3575.
- [45] Y. S. Park, S. Y. Yoon, J. S. Park, J. S. Lee, *NPG Asia Mater.* **2016**, *8*, e249.
- [46] W. Hällström, T. Mårtensson, C. Prinz, P. Gustavsson, L. Montelius, L. Samuelson, M. Kanje, *Nano Lett.* **2007**, *7*, 2960.
- [47] K. Adolfsson, H. Persson, J. Wallentin, S. Oredsson, L. Samuelson, J. O. Tegenfeldt, M. T. Borgström, C. N. Prinz, *Nano Lett.* **2013**, *13*, 4728.
- [48] G. Hammarin, H. Persson, A. P. Dabkowska, C. N. Prinz, *Colloids Surf., B* **2014**, *122*, 85.
- [49] R. Hückelhoven, *Annu. Rev. Phytopathol.* **2007**, *45*, 101.
- [50] J. Mansfield, S. Genin, S. Magori, V. Citovsky, M. Sriariyanum, P. Ronald, M. Dow, V. Verdier, S. V. Beer, M. A. Machado, I. Toth, G. Salmond, G. D. Foster, *Mol. Plant Pathol.* **2012**, *13*, 614.
- [51] Y. L. Ong, A. Razatos, G. Georgiou, M. M. Sharma, *Langmuir* **1999**, *15*, 2719.
- [52] B. Maier, L. Potter, M. So, H. S. Seifert, M. P. Sheetz, *Proc. Natl. Acad. Sci. USA* **2003**, *100*, 16012.
- [53] P. H. Tsang, G. Li, Y. V. Brun, L. B. Freund, J. X. Tang, *Proc. Natl. Acad. Sci. USA* **2006**, *103*, 5764.
- [54] I. Schoen, W. Hu, E. Klotzsch, V. Vogel, *Nano Lett.* **2010**, *10*, 1823.
- [55] K. A. Kline, S. Fälker, S. Dahlberg, S. Normark, B. Henriques-Normark, *Cell Host Microbe* **2009**, *5*, 580.
- [56] J. Sjollem, H. C. van Der Mei, C. L. Hall, B. W. Peterson, J. de Vries, L. Song, E. D. D. Jong, H. J. Busscher, J. J. T. M. Swartjes, *Sci. Rep.* **2017**, *7*, 4369.
- [57] H. C. Flemming, J. Wingender, *Nat. Rev. Microbiol.* **2010**, *8*, 623.
- [58] G. S. Lorite, R. Janissen, J. H. Clerici, C. M. Rodrigues, J. P. Tomaz, B. Mizakoff, C. Kranz, A. A. de Souza, M. A. Cotta, *PLoS One* **2013**, *8*, e75247.
- [59] R. Janissen, D. M. Murillo, B. Niza, P. K. Sahoo, M. M. Nobrega, C. L. Cesar, M. L. A. Temperini, H. F. Carvalho, A. A. de Souza, M. A. Cotta, *Sci. Rep.* **2015**, *5*, 9856.
- [60] E. Stokstad, *Science* **2015**, *348*, 620.
- [61] A. Abbott, *Nature* **2017**, *546*, 193.
- [62] L. S. Muranaka, T. E. Giorgiano, M. A. Takita, M. R. Forim, L. F. C. Silva, H. D. Coletta-Filho, M. A. Machado, A. A. de Souza, *PLoS One* **2013**, *8*, e72937.
- [63] T. Mårtensson, P. Carlberg, M. Borgström, L. Montelius, W. Seifert, L. Samuelson, *Nano Lett.* **2004**, *4*, 699.
- [64] M. T. Borgström, J. Wallentin, J. Trägårdh, P. Ramvall, M. Ek, L. R. Wallenberg, L. Samuelson, K. Deppert, *Nano Res.* **2010**, *3*, 264.
- [65] G. Cao, *Nanostructures & Nanomaterials: Synthesis, Properties & Applications*, Imperial College Press, London **2004**.
- [66] M. Shaat, A. Abdelkefi, *J. Appl. Phys.* **2016**, *120*, 235104.
- [67] W. Hallstrom, M. Lexholm, D. B. Suyatin, G. Hammarin, D. Hessman, L. Samuelson, L. Montelius, M. Kanje, C. N. Prinz, *Nano Lett.* **2010**, *10*, 782.
- [68] M. Dunaevskiy, P. Geydt, E. Lähderanta, P. Alekseev, T. Haggrén, J. P. Kakko, H. Jiang, H. Lipsanen, *Nano Lett.* **2017**, *17*, 3441.
- [69] T. Beléndez, C. Neipp, A. Beléndez, *Eur. J. Phys.* **2002**, *23*, 317.
- [70] H. Persson, C. Købler, K. Mølhave, L. Samuelson, J. O. Tegenfeldt, S. Oredsson, C. N. Prinz, *Small* **2013**, *9*, 4006.
- [71] L. D. Landau, E. M. Lifshitz, *Theory of Elasticity*, Pergamon Press, New York **1959**.
- [72] C. L. Dos Santos, P. Piquini, *Phys. Rev. B* **2010**, *81*, 75408.
- [73] M. J. Davis, W. J. French, N. W. Schaad, *Curr. Microbiol.* **1981**, *6*, 309.
- [74] B. Niza, H. D. Coletta-Filho, M. V. Merfa, M. A. Takita, A. A. de Souza, *Plant Pathol.* **2015**, *64*, 1259.
- [75] C. A. Schneider, W. S. Rasband, K. W. Eliceiri, *Nat. Methods* **2012**, *9*, 671.
- [76] S. Stallinga, B. Rieger, *Opt. Express* **2010**, *18*, 24461.
- [77] U. Rabe, K. Janser, W. Arnold, *Rev. Sci. Instrum.* **1996**, *67*, 3281.
- [78] R. B. Bhiladvala, Z. J. Wang, *Phys. Rev. E: Stat., Nonlinear, Soft Matter Phys.* **2004**, *69*, 36307.
- [79] D. W. Allan, *Proc. IEEE* **1966**, *54*, 221.
- [80] F. Czerwinski, A. C. Richardson, L. B. Oddershede, *Opt. Express* **2009**, *17*, 13255.
- [81] R. M. A. Sullan, A. Beaussart, P. Tripathi, S. Derclay, S. El-Kirat-Chatel, J. K. Li, Y.-J. Schneider, J. Vanderleyden, S. Lebeer, Y. F. Dufrêne, *Nanoscale* **2014**, *6*, 1134.
- [82] S. Y. Quah, S. Wu, J. N. Lui, C. P. Sum, K. S. Tan, *J. Endod.* **2012**, *38*, 81.
- [83] A. Olofsson, M. Hermansson, H. Elwing, *Appl. Environ. Microbiol.* **2003**, *69*, 4814.
- [84] S. C. Picchi, M. A. Takita, H. D. Coletta-Filho, M. A. Machado, A. A. de Souza, *Plant Pathol.* **2016**, *65*, 561.
- [85] Z. Li, H. Persson, K. Adolfsson, L. Abariute, M. T. Borgström, D. Hessman, K. Åström, S. Oredsson, C. N. Prinz, *Nanoscale* **2017**, *9*, 19039.
- [86] S. Chatterjee, R. P. P. Almeida, S. Lindow, *Annu. Rev. Phytopathol.* **2008**, *46*, 243.
- [87] L. Gao, Y. Cui, J. Wang, A. Cavalli, A. Standing, T. T. T. Vu, M. A. Verheijen, J. E. M. Haverkort, E. P. A. M. Bakkers, P. H. L. Notten, *Nano Lett.* **2014**, *14*, 3715.
- [88] R. Caserta, M. A. Takita, M. L. Targon, A. P. De Souza, L. Peroni, A. Andrade, C. A. Labate, E. W. Kitajima, M. A. Machado, A. A. De Souza, D. De Gene, *Appl. Environ. Microbiol.* **2010**, *76*, 4250.



Supporting Information

for *Small Methods*, DOI: 10.1002/smt.201700411

Nanowire Arrays as Force Sensors with Super-Resolved
Localization Position Detection: Application to Optical
Measurement of Bacterial Adhesion Forces

*Aldeliane M. da Silva, Prasana K. Sahoo, Alessandro Cavalli,
Alessandra A. de Souza, Erik P. A. M. Bakkers, Carlos L.
Cesar, Richard Janissen,* and Monica A. Cotta**

Supporting Information

Nanowire arrays as Force Sensors with Super Resolved Localization Position Detection: Application to Optical Measurement of Bacterial Adhesion Forces

Aldeliane M. da Silva, Prasana K. Sahoo, Alessandro Cavalli, Alessandra A.de Souza, Erik P.A.M.

Bakkers, Carlos L. Cesar, Richard Janissen*, Monica A. Cotta*

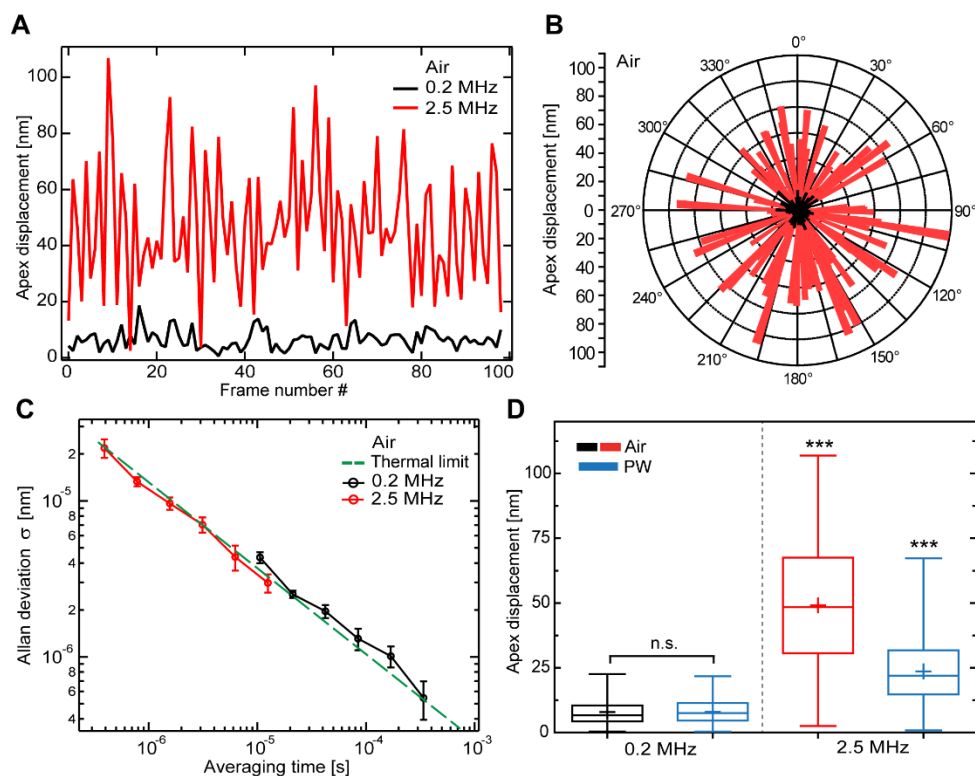


Figure S1: (A) Apex displacements values, obtained from center localization using Gaussian fitting for sequential video frames, for measurements with different pixel net frequencies (0.2 and 2.5 MHz). (B) Polar plot provides displacement magnitudes and bearings. (C) Allan deviation plot exhibit that the thermal limit is reached for both measurements. (D) One-way ANOVA and comparison via Tukey post-hoc test with $p = 0.0001$ were carried out for statistical analysis. Tukey box plot shows significant differences only for measurements at higher pixel net frequencies.

Supplemental Video S2: Confocal fluorescence time lapse microscopy (left) of single nanowire-attached *X. fastidiosa* bacterial cells released (right) upon NAC exposure.

Supplemental Video S3: Confocal fluorescence time-lapse microscopy of individual *X. fastidiosa* cells firmly attached to nanowire arrays.

Supplemental Video S4: Confocal fluorescence time-lapse microscopy (left) of large *X. fastidiosa* bacterial cluster (right: cluster volume rendering) released from nanowire arrays upon NAC exposure.